Title of thesis: **SIMULATION EFFECT OF HOT GAS IMPINGEMENT ON NACELLE LIP SKIN**

Date of submission (Academic year): **7/6/2017 (2016/2017)**

Candidate Matrix no: **120388**

Name of supervisor: **Dr. Mohd Azmi Ismail**

## DECLARATION

This work has not previously been accepted in substance for any degree and is not being concurrently submitted in candidature for any degree.

Signed …… (Mohammad Harith Yaccob Bin Syed)

Date ……

**Statement 1**

This thesis is the result of my own investigation, except where otherwise stated. Other sources are acknowledged by giving explicit references. Bibliography/references are appended.

Signed …… (Mohammad Harith Yaccob Bin Syed)

Date ……

**Statement 2**

I hereby give consent for my thesis, if accepted, to be available for photocopying and for interlibrary loan, and for the title and summary to be made available outside organizations.

Signed …… (Mohammad Harith Yaccob Bin Syed)

Date ……

## ACKNOWLEDGEMENT

First and foremost, I would like to express my deepest gratitude to my supervisor, Dr. Mohd Azmi Ismail for all his guidance that helped me to finish this project successfully. He has guided me and offered tips that helped me to do Ansys Fluent simulation. In addition to that, special thank goes to him for all the encouragement that he has given to me through the ups and downs of this project and enables me to complete this final year project successfully and smoothly.

Next, special thank goes to team CAD-IT Consultants in which their team has conducted Ansys workshop that has helped me to understand the principles underlying behind Ansys calculations especially Ansys CFD and Ansys Mechanical. Not to forget, En. Muhammad Nurfazli from CAD-IT Consultants where he has conducted a private consultation session with me to offer me some advice regarding my project.

I would also like to express my gratitude to Dr. Abdullah Aziz Saad and Dr. Mohamad Aizat Abas for their consultation regarding fluid structure interaction and also on stress strain distribution on the lip skin in which has helped me to understand the basic mathematics and formula used in FSI simulation and better understanding on stress strain distribution.

Last but not least, my special thanks goes to my father, Syed Bin M.Mohamad, my mother, Marzidah Binti Mohammad for their morale support and words of encouragement that has helped to keep my morale high throughout this project.

**TABLE OF CONTENTS**

## LIST OF FIGURES

## LIST OF SYMBOLS

| | | |
|---|---|---|
| $Re_G$ | = | Reynolds Number for the surface area of impingement |
| $Nu_{ave}$ | = | Average Nusselt number |
| $h_{ave}$ | = | Average heat transfer coefficient |
| $Cx$ | = | Distance between the two nozzle |
| $d$ | = | Diameter of the nozzle |
| $Pr$ | = | Prandtl number |
| $k$ | = | Air thermal conductivity |
| $q_{lip\text{-}skin}$ | = | Rate of heat transfer on the impingement area |
| $A_{impingement}$ | = | Area of effective impingement |
| $T_{piccolo}$ | = | Temperature of the air inside piccolo tube |
| $T_{avg\ impingement}$ | = | Average temperature on the effective impingement area |
| $G$ | = | Ratio of hot gas mass flow rate to area of effective impingement |
| $\mu$ | = | Dynamic viscosity of air |
| $\sigma_e$ | = | Equivalent stress (von Misses) |
| $\varepsilon^{th}$ | = | Thermal strain |

**ABSTRAK**

Pengumpulan ais semasa penerbangan melibatkan pengumpulan ketulan ais pada kulit bibir nasel di enjin pesawat. Pengumpulan ais di permukaan dalaman kulit bibir nasel boleh membawa padah kepada mana-mana pesawat yang terbang [2]. Aplikasi pengkomputeran dinamik bendalir (CFD) telah digunakan secara meluas untuk mengkaji kesan pengumpulan ais di atas kulit bibir nasel. Di dalam kajian ini, interaksi antara bendalir dan struktur telah digunakan untuk mengkaji kesan hentaman gas panas pada kulit bibir nasel terhadap sifat haba bahan. Kajian ini telah mendapati bahawa bahan yang digunakan untuk kajian ini iaitu AL 1 siri, 2 siri dan 7 siri mempunyai tingkah laku yang bergantung kepada suhu. Ianya berkait rapat dengan ciri-ciri mikroskopik nereka. Kajian ini telah menunjukkan bahawa kekuatan tegangan bahan berkurang apabila suhu bertambah dan kajian ini turut membuat kesimpulan bahawa aluminum 7 siri adalah bahan yang paling sesuai digunakan untuk bahan kulit bibir nasel.

**ABSTRACT**

Ice accumulation during flight includes the accumulation of icing on the nacelle lip skin of the aircrafts engines. The accumulation on the ice on the inner surface of the lipskin can be hazardous to any flying aircraft [2]. Computational Fluid Dynamics (CFD) has been widely used to study the effect of ice accretion onto the nacelle lip skin. This study however utilizes the fluid structure interaction (FSI) to study the effect of hot gas impingement on the nacelle lip skin towards the thermal properties of the material. It was found that the material used for this study, AL 1 series, 2 series and 7 series has a temperature dependent behavior which is closely related to their microscopic properties. This study has shown that the tensile strength of the materials decreases as the temperature increases and this study also has concluded that aluminum 7 series is the most suitable material to be used for the nacelle lip skin material

**PAPER FORMAT**

This journal paper is organized into 4 sections as listed below:

a) Part 1.0 is the introduction for this study. In this section, the literature on current study on nacelle lip skin, the introduction to this study, problem statement and objective of this study were stated.

b) Part 2.0 is the methodology used for this study. This part was divided into 4 different subsection outlining the steps taken from start to finish that was involved and related with this study. This sections also discusses the CFD tool used for this study as well as the pre-processor software used which was the Gambit.

c) Part 3.0 is outlines the results and discussions for this study. In this section, all the data analysis obtained from this study was presented in graphical and figure form. This includes the discussion for the data. The tabulation of data however was presented in the appendices in table 2.1, 3.1 and also 3.2.

d) Part 4.0 is where the conclusion obtained from this study was stated. The objectives of the study was answered in this section.

## 1.0: INTRODUCTION

Aircraft icing is the accretion of supercooled liquid which form on aircraft during the flight. Accretion of ice onto vital parts of the aircraft components can bring adverse effect to the flight performance and conditions.[1]

Ice accumulation during flight includes the accumulation of icing on the nacelle lip skin of the aircraft engines. These accumulation of ice on the inner surface of the lip skin can be hazardous to flying aircrafts. Therefore, it is very important for any aircraft to be installed with anti-icing system. Ice accumulation on nacelle lip skin can possesses a major problem on any flying aircraft as it greatly alters the aerodynamic properties of the aircraft which in turn can lead to higher fuel consumption due to increased drag force generated by the non-aerodynamic shape present on the lip skin. [2]

There are many type of aircraft anti icing system which are now commercially used. One of the good example and most used anti icing system is the Piccolo Tube Anti Icing (PTAI). Piccolo tube, with a series of in line and staggered holes, is placed inside the wing leading edge and near to its surface. Hot air is then bled from the aircraft's engine compressor and passed through the piccolo tube and it ejects from the piccolo tube holes in the form of high velocity jet, which impinges on the inner surface of the wing leading edge. Heat conduction from the inner surface to outer surface then results in maintaining the temperature of the outer surface leading edge to avoid any ice formation on the surface. [3]

The hot air that impinges on the nacelle lip skin may have an effect on the thermal and mechanical properties of the nacelle lip skin. Rapid heat transfer from the piccolo tube onto the nacelle lip skin will cause the temperature of the lip skin to increase rapidly. Although this

phenomena is important to degrade the ice formed on the surface of the lip skin, it possesses an effect to the material of the nacelle lip skin which will alter the mechanical properties of the lip skin.

The variation in mechanical properties can pose a direct threat to nacelle lip skin as when it deforms, it will alters the original shape of the lip skin resulting a significant change in aerodynamic properties of the geometry. Hence it is vital to study the effect of hot gas flow from PTAI in term of material deformation and thermal stress on the nacelle lip skin so we can predict the nacelle lip skin life expectancy.

Computational Fluid Dynamic (CFD) is a useful tool to be used in studying the deformation and properties change of the lip skin. CFD has been widely used by researchers to predict heat transfer, fluid flow and also combustion. In this study, Ansys FLUENT will be used as the CFD tool. Additionally, to find the mechanical deformation, the FLUENT will be paired with Static Structural. This method is called as fluid structure interaction (FSI).

Current and latest research by Stefan Kennedy, Theresa Robinson and Stephen Spence from Queen's University Belfast suggested that the lip skin deformation can cause a distortion of the flow field at the fan face which can in turn degrade the engine performance and lead to compressor surge. Nonetheless, this paper only discusses about the damage to the nacelle lip skin caused by external factors weather during taxing, climb or cruise. The damage studied in this paper is due to bird strike during flight, debris on the runway during take-off and landing and other impact during parking or taxiing. [4]

In PTAI system, hot air is bled from the engine compressor at high pressure and temperature and were conducted forward to the fixed leading edge at various free stream Mach number as well

as ambient temperatures. The high pressure and high temperature air exits the piccolo tube via a series of holes or nozzles strategically drilled to generate a series of high velocity jets of hot air which will impinge on the inner surface of D-chamber. [2]

The predicted results (figure 1.1) show that the upper half of the lip skin sees lower temperature than the lower half. The highest temperature spots occur at the points where the high velocity jets form the nozzles impinge directly on the lower half of the lip skin which will also be referred as effective impingement area $A_{impingement}$. During flight, this portion of the lip-skin is needed to be cleared from ice in order to avoid ice shedding and subsequently lead to ice ingestion by the engine [2].

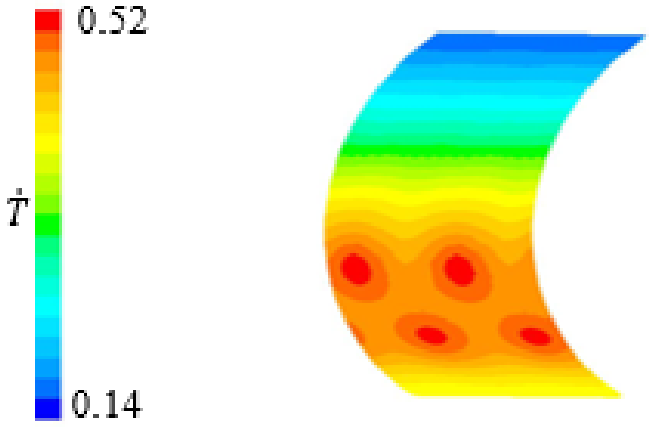


Figure 1.1: The temperature contour on the nacelle lip skin in Taxi test at $Re_{PTAI}$ of 34,000 [2]

Using Fluid Structure Interaction (FSI), the objective of this study is to determine the thermal characteristics. The thermal stress and strain caused by the hot gas from PTAI also will be determined and will be compared between three different type of aluminium which are 7 series, 2 series and 1 series.

## 2.0: METHODOLOGY

### 2.1 Geometry

First of all, the geometry was drawn using Gambit pre-processor before importing it into Workbench. The geometry used in this study is as shown in figure 2.1 and 2.2. Note the diameter, d in this study is 2mm.

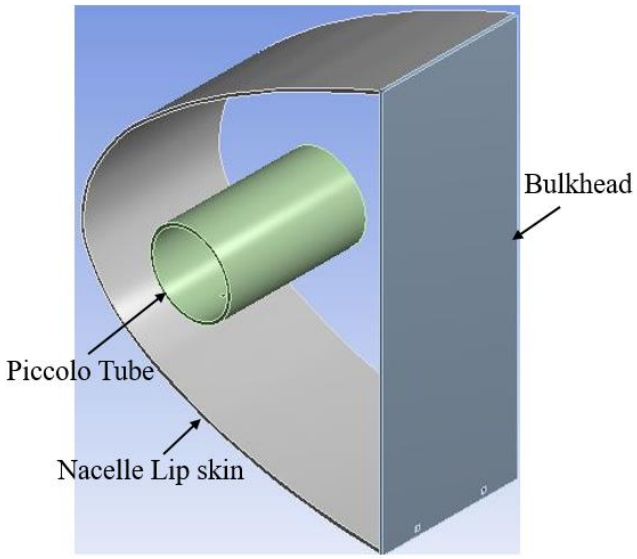


Figure 2.1: Overall geometry of nacelle lip skin

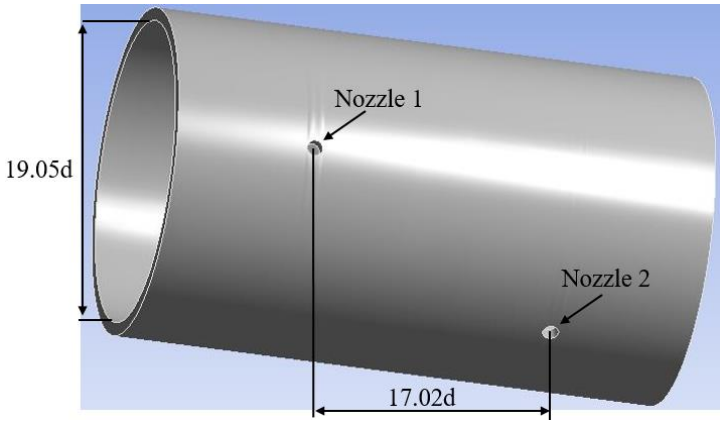


Figure 2.2: Details of piccolo tube showing nozzle 1 and 2

The geometry drawn in Gambit pre-processor accounts for the fluid domain and as well as solid domain (figure 2.3).

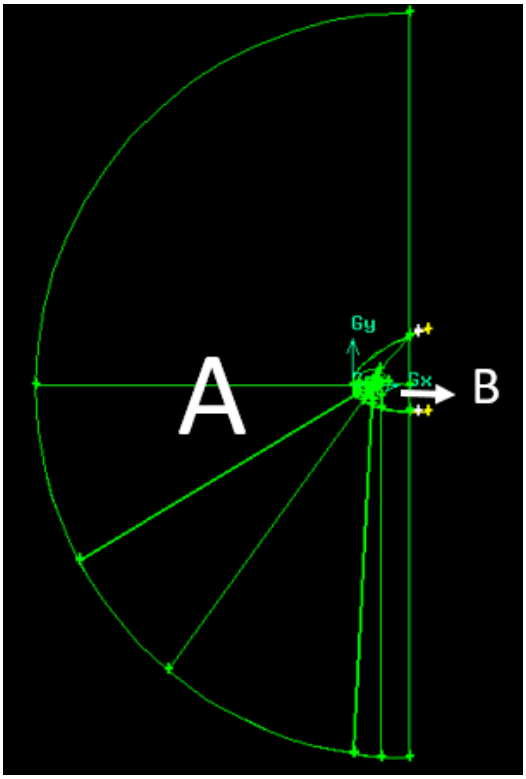


Figure 2.3: Labelled A is the fluid domain in semi-circular shape while B represents the nacelle lip skin with piccolo tube.

Referring to figure 2.3, it is seen that the fluid domain only account for the frontal side of the nacelle lip skin. This is due to the nature of this project that only study about the fluid that comes from the environment and during actual flight, the fluid that affect the outcome of this study is only on the area of the semicircular fluid domain or the frontal area of the nacelle lip skin.

**2.2 Meshing and Boundary Conditions**

Using Gambit pre-processor, the mesh was created which includes naming the surface and boundary conditions for the faces. More than $2.9 \times 10^6$ linear hexahedron elements were used for

the model (figure 2.4). Note that the area around piccolo tube and lip-skin has a finer mesh to provide higher accuracy of result for the simulation.

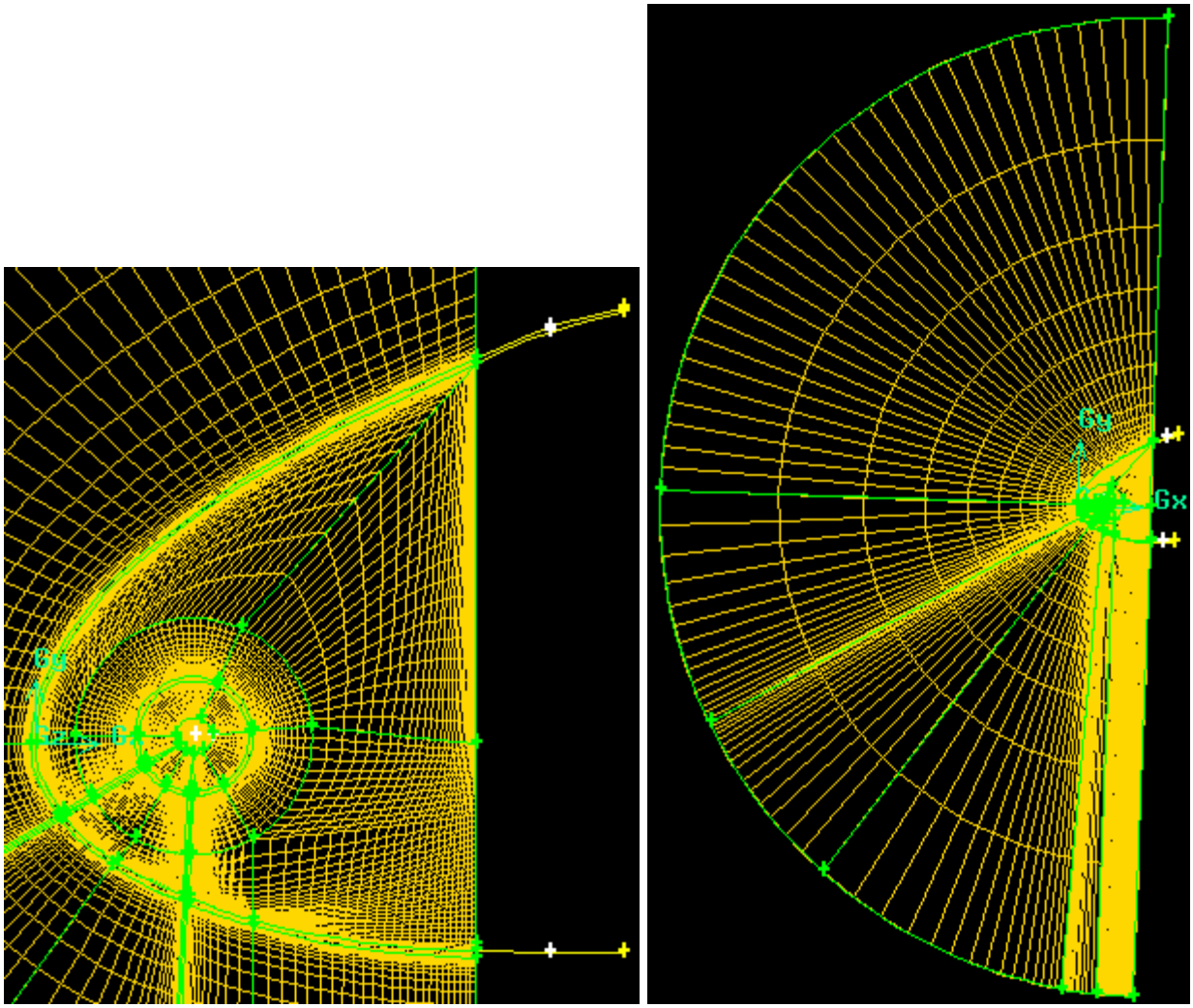


**(a)** **(b)**

Figure 2.4: (a) Fine mesh around the piccolo tube and the lip skin. (b) The full mesh generated on the fluid and solid domain in Gambit pre-processor for the geometry

For boundary condition, pressure far field with 0.1 Mach number was used on the outer surface of the nacelle lip skin. Periodic boundary conditions were used on the right and left side of the nacelle lip skin and piccolo tube. This is because periodic boundary condition is the most

suitable boundary condition to be used since the both end of lip skin and tube are exposed to ambient and periodic boundary condition approximates a large system using a unit cell.

Other boundary condition includes the inlet for hot gas which is called hot gas in and outlet for the hot gas which is called hot gas out. Referring to figure 2.5, showing the hot gas outlet or exhaust (in red circle) which is located on lower part of the bulkhead.

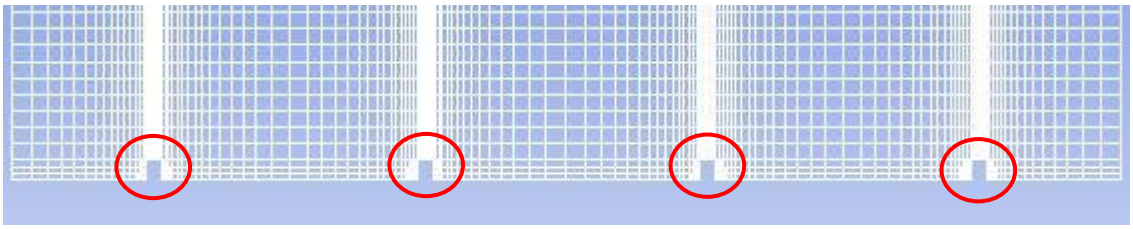

Figure 2.5: The exhaust (in red circle) at the lower part of bulkhead

**2.3 Ansys FLUENT Simulation**

The geometry drawn in Gambit pre-processor was imported into Ansys FLUENT for CFD simulation. The simulation uses turbulent model which are the shear-stress transport (SST) k-ω model and also the energy equation. SST k-ω model is an effective and accurate formulation of the k-ω model in far field. The SST model incorporates a damped cross diffusion derivative term in the ω equation. Hence SST k-ω are able to provide a better accuracy of simulation result [5].

The boundary values are then inserted. For the pressure far field, turbulence intensity (constant) was specified at 2% and the operating conditions are at 68051.25 Pa. As for hot gas in and hot gas out boundary, the turbulent intensity was set at 5% intensity and operates at same operating conditions as pressure far field.

Next, the value of the parameter to be studied, the mass flow rate of the hot gas in, was specified in the boundary. The value of the mass flow rate and Reynolds number $Re_G$ used in this study can be referred to table 2.1 in appendix.

The calculation were initiated with the first 1000 iterations using first order upwind, and the last 1000 iterations using second order upwind. This method of using second order upwind in simulation helps this study to obtain a better accuracy of results. The solution fully converges after 2000 iterations.

**2.4 Finite Element Modeler and Static Structural**

In order to import the geometry and meshing into Ansys mechanical, Finite Element Modeler (FEM) system was used. The geometry that was imported into FEM system only involves the solid domain which are the nacelle lip skin and piccolo tube. The geometry and meshing is shown in figure 2.6 below. Note that the imported mesh is the same as the mesh found in FLUENT simulation.

Finite element modeler was developed to handle some of the mesh based capabilities found in mechanical APDL that cannot be read by Ansys Mechanical.

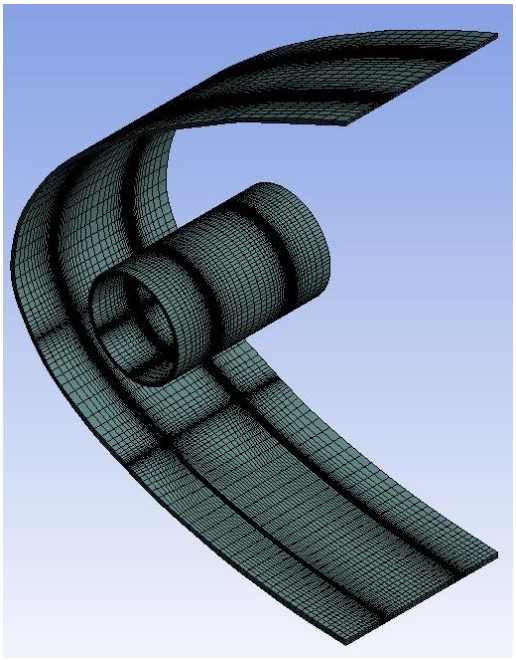

Figure 2.6: Nacelle lip skin and piccolo tube meshing in FEM

Contrary with Ansys FLUENT, in static structural, the geometry does not involve any fluid domain and solely depends on the solid domain alone. However since we are using the FSI method, the result in CFD simulation will affect the result in static structural.

All the material data for Aluminum 7075-T6 series, 2024-T4 series and 1100-O series were input into the engineering data cell.

The temperature of the geometry obtained from the CFD simulation were imported into static structural. Using this imported body temperature, mechanical analysis was conducted. The parameter that is studied in static structural is the thermal stress and also the strain.

**2.5: Materials Used for This Study**

For this project, the material used and their composition are as follow:

AL 1100-O: 99% Al, 0.12 Cu, Annealed

AL 2024-T4: 93.5% Al, Cu 4.4,  Mn 0.6, Mg 1.5, Heat treated and naturally aged

AL 7075-T6: 90% Al, Zn 5.6, Mg 2.5, Cu 1.6, Cr 0.23, Heat treated and artificially aged

The mechanical properties for all the material inserted into Ansys Mechanical is shown in table 2.2 in the appendices.

## 3.0: RESULTS AND DISCUSSION

### 3.1 Result Verification

For this study, the CFD simulation results obtained was compared with the study conducted by Brown [6]. Figure 3.1 below shows the correlation obtained for this study compared with Brown's correlation.

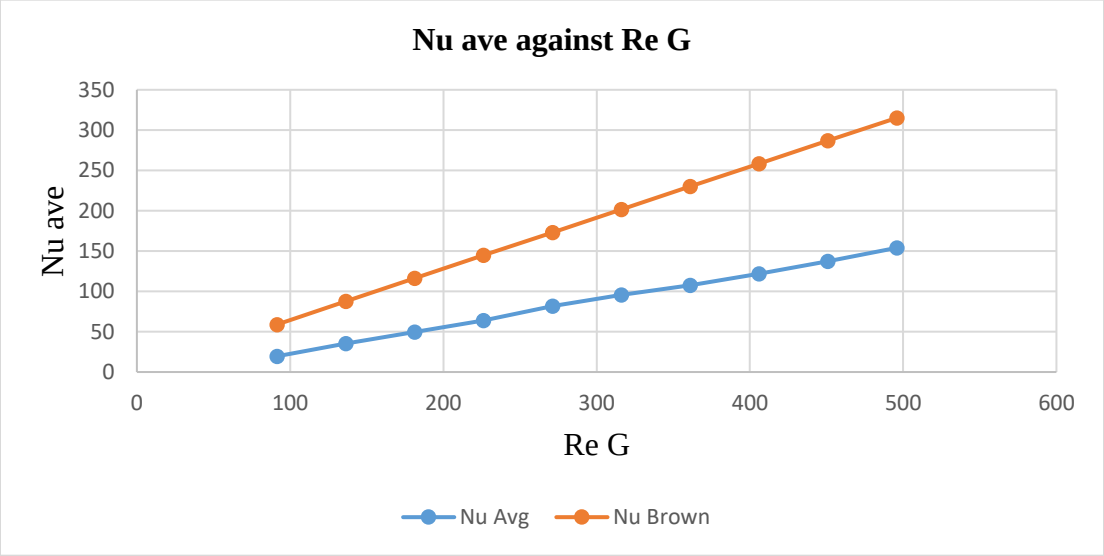


Figure 3.1: Correlation between Brown and this study correlation

From figure 3.1, we can see that there is slight difference between Brown's correlation [6] and the result obtained in this study. Brown uses the following equation to estimate Nusselt number:

$$Nu_{ave} = 0.577\ Re_G^{0.922}\ (\frac{Cx}{d})^{0.064}\ Pr^{0.3} \quad (1)$$

For this study, the following correlation were used:

$$Nu_{ave} = \frac{h_{ave}d}{k} \quad (2)$$

$h_{ave}$ was determined using the following formula:

$$h_{ave} = \frac{q_{lip-skin}}{(A_{immpingement}\,(T_{piccolo} - T_{avg\ impingement}))} \quad (3)$$

From figure 3.1, we see that the results obtained in this study has lower gradient and has the same trend as Brown's correlation, which is the average Nusselt number increases proportionally with the Reynolds number.

For this study, the conditioned the lip skin studied is during the cruise altitude. Cruise altitude for commercial plane which are at 20,000 ft to 35,000 ft typically has the ambient air temperature of around -20 to -30 ℃. Hence a rapid heat transfer from the heated surface of nacelle lip skin to the ambient air happens.

From equation 3, we know that $h_{ave}$ is inversely proportional to the $T_{avg\ impingement}$ if all the other parameter in the same equation is kept constant. Hence the heat transfer from the heated nacelle lip-skin to the ambient air causes a drop in the $T_{avg\ impingement}$. This has consequently cause a drop in the calculated $h_{ave}$.

Relating this to equation 2, the average Nusselt number $Nu_{ave}$, will drop if the $h_{ave}$ drop or if the ambient air drop. The table of data obtained from CFD simulation which was used for the calculation that lead to figure 3.1 is shown in table 2.1. Note that the Reynolds number was calculated using the following relation:

$$Re_G = \left(\frac{4Gd}{\pi\mu}\right) \quad (4)$$

### 3.2: Ansys Mechanical Solver

For this study, structural results was used to yield a desirable result. This is because equivalent stress allows any arbitrary three-dimensional stress state to be represented as a single positive stress value. Equivalent stress also is part of the maximum equivalent stress failure theory used to predict yielding in a ductile material [7]. For the stress analysis, the equivalent (von Mises) stress was used.

$$\sigma_e = \left[\frac{(\sigma_1 - \sigma_2)^2 + (\sigma_2 - \sigma_3)^2 + (\sigma_3 - \sigma_1)^2}{2}\right] \quad (5)$$

For the strain analysis, thermal strain was computed and used because there is a temperature load on the body of geometry. The equation used by Ansys Mechanical to solve is as follow:

$$\varepsilon^{th} = \alpha^{se}\left(T - T_{ref}\right) \quad (6)$$

$T_{ref}$ is also the reference temperature which are used to specify the reference temperature as a material property for cases where the temperature is different [7].

### 3.3: Stress And Strain Analysis for Different Temperature on the Impingement Area

After the simulation was conducted, The temperature contour obtained from CFD simulation were also shown below in figure 3.2 and the average thermal stress and thermal strain on the effective impingement area was obtained and the results obtained are shown in figure 3.3.

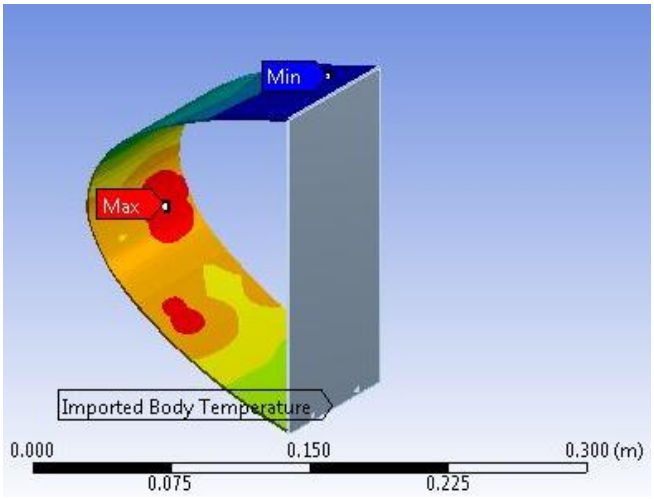


Figure 3.2: Temperature contour obtained from CFD simulation for $Re_G$ = 0.013629447 Kg/s

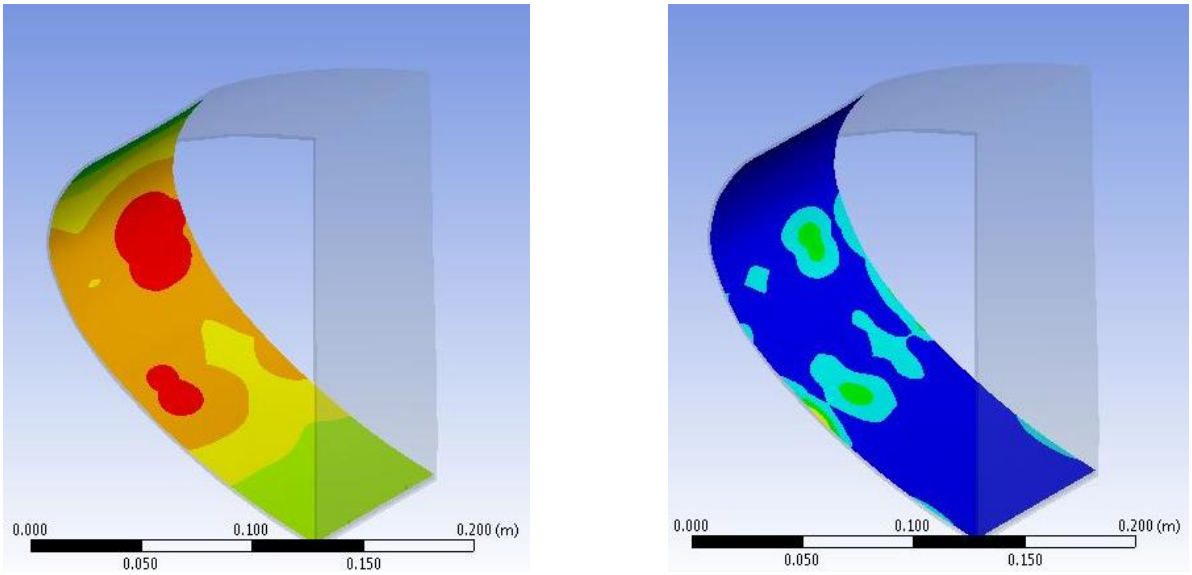


(i) (ii)

Figure 3.3: (i) Thermal strain contour and (ii) Thermal stress contour on nacelle lip skin for AL 1 series at $Re_G$ = 0.013629447 Kg/s

Figure 3.2 shows the temperature contour that was obtained from CFD simulation and imported into Ansys mechanical. The highest temperature region is at the location of the nozzle where the lip skin experience highest temperature. This pattern is consistent with figure 3.3, where

the highest thermal strain and thermal stress exerted by the nacelle lip skin is at the location where the nozzle is. This is where the temperature is the highest since the nozzle from piccolo tube is the pressure outlet for the hot gas. The area where the hot gas impinges or the thermal stress and thermal strain is the highest is also called as effective impingement area. The data of stress and strain obtained from Ansys Mechanical is recorded and a series of graph were plotted to gain better understanding as shown in figures below (figure 3.4, 3.5, 3.6 and 3.7).

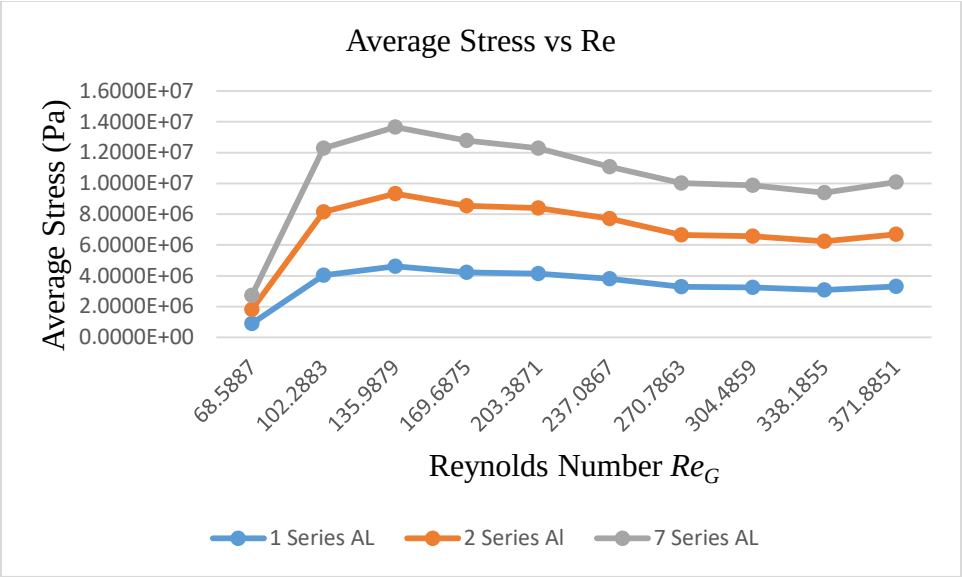


Figure 3.4: Graph of average stress against Reynolds number $Re_G$ for all the Aluminum series

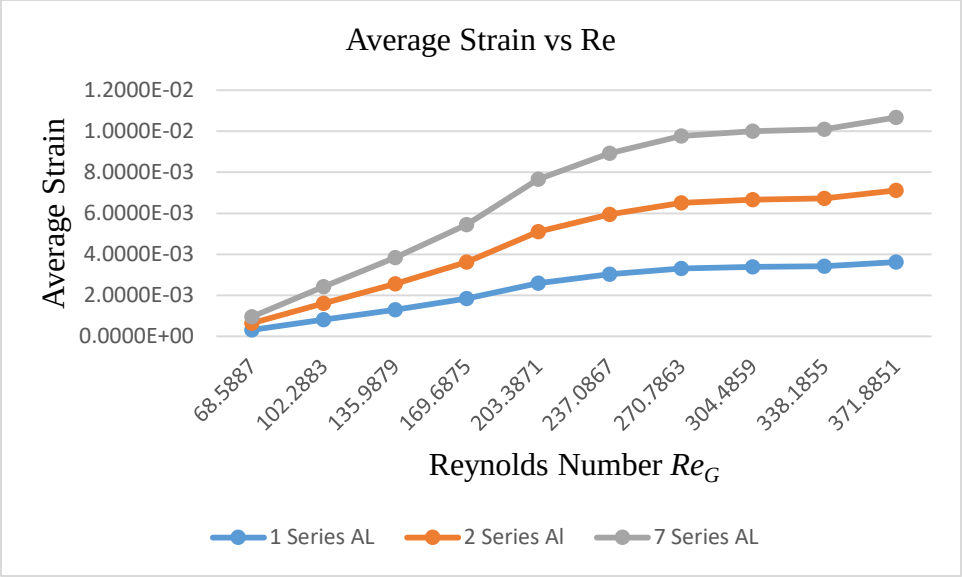


Figure 3.5: Graph of average strain against Reynolds number $Re_G$ for all Aluminum series

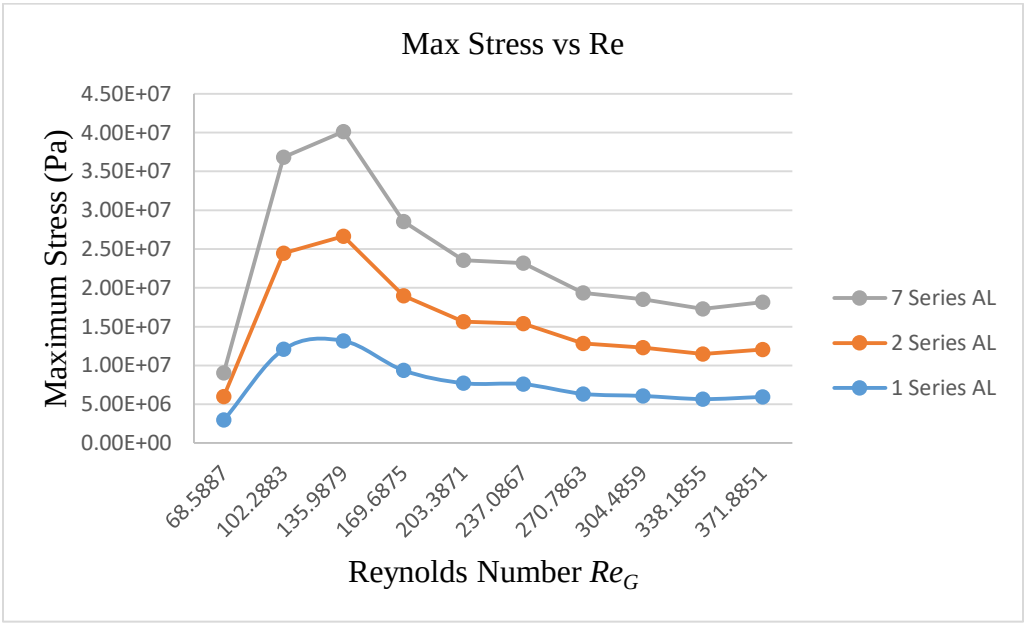


Figure 3.6: Graph of maximum stress against Reynolds number $Re_G$ for all Aluminum series

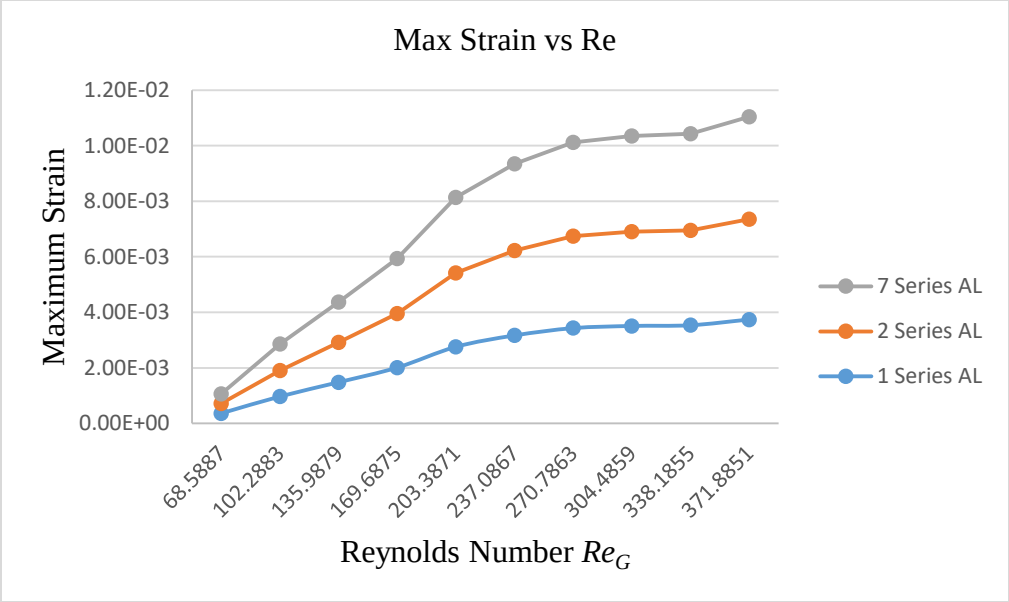


Figure 3.7: Graph of maximum strain against Reynold Number $Re_G$ for all Aluminum series

The tables of data obtained for average stress (Pa), average strain on the effective impingement area as well as maximum stress and maximum strain can be referred to table 3.1 in appendices.

From figure 3.4, we can see that the average stress on the effective impingement area increases steadily until it reaches $Re_G$ = 135.988 which at this point, the average stress for all the Aluminum series is highest. From figure 3.4 also, we see that the all the Aluminum series shows a same trend and behavior across the various $Re_G$. After it reaches their highest average stress, as the $Re_G$ is further increased, the average stress for all the aluminum start to decrease slowly.

Figure 3.5 on the other hand, shows the average strain on impingement area which also have a same trend for all the Aluminum series across various $Re_G$. The graph for all the aluminum series shows a steady increase until they reaches their highest strain at $Re_G$ = 337.8851.

The same trend for stress and strain can also be observed on the maximum stress and maximum strain graph against $Re_G$. Figure 3.6 and 3.7 shows the same trend as figure 3.4 and 3.5. The aluminum 7 series has shown us that it exerts higher stress and strain.

To analyse further and correlate with the figures above, the effect of temperature and the rate of stress and strain was plotted with graph as shown in figure 3.8 and figure 3.9. The data for the maximum temperature is shown in table 3.2 in appendices.

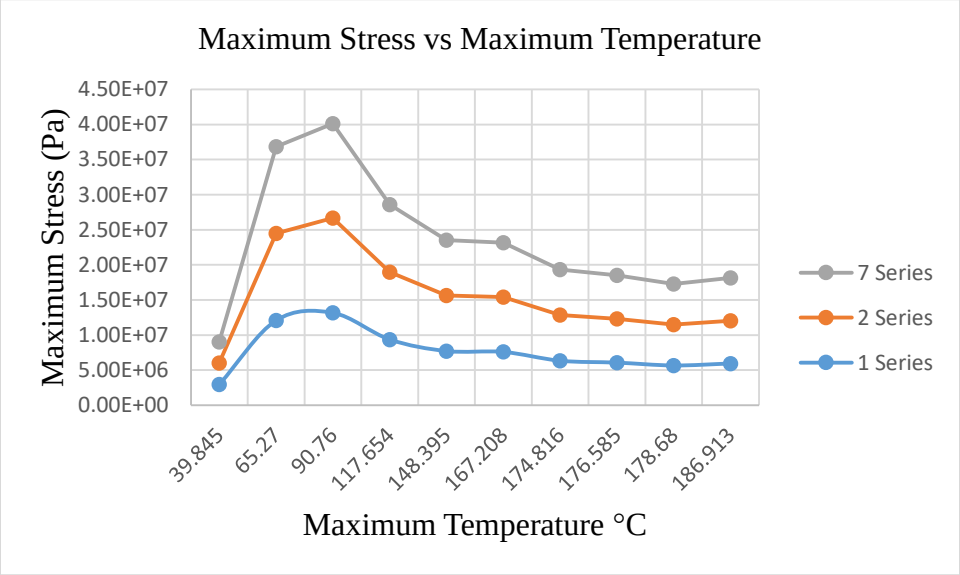


Figure 3.8: Graph of maximum stress against maximum temperature

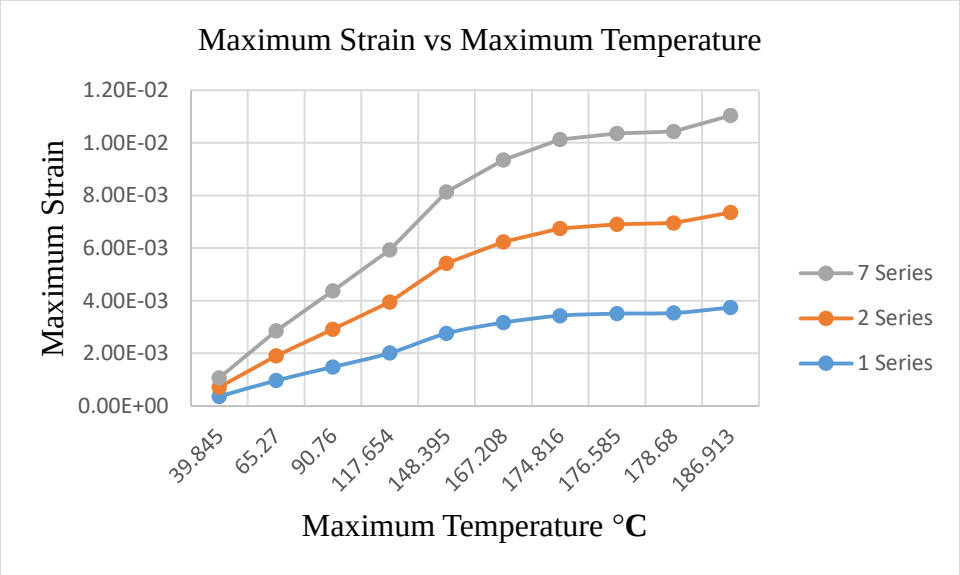


Figure 3.9: Graph of maximum strain against maximum temperature

From figure 3.8, we can see that after reaching the maximum stress at 90.76 °C, the stress begins to decrease steadily. Different case can be observed on figure 3.9 where the maximum strain increases steadily until it reaches maximum temperature at 186.913°C which is at the $Re_G$ = 337.8851. The result obtained in shows the influence of temperature on the stress curve of a material. We can observe that the stress decreases with increase in temperature for all type of aluminum series. It is obvious that the material has reached their ultimate tensile strength at $Re_G$ = 135.98 and is plastically deformed after that limit. Plastic deformation is the breaking of atomic bonds by the dislocation movement. At elevated temperature, the process of atomic bonds breakage is accelerated. As the temperature rises, the atoms in the material gain more kinetic energy and vibrates higher. The increased vibration in turn causes the atoms to slip to new locations in the material. This is what induces the material to deform plastically.

The results obtained in this study is expected as materials will show different properties at elevated temperature. While strain continues to increase with increasing temperature, the stress

began to reduce as the temperature goes higher. It is observed that the material properties depends strongly on the temperature it is exerted.

The findings of this study is consistent with the findings obtained by reference [8] where their experimental data were shown in figure 3.10 below.

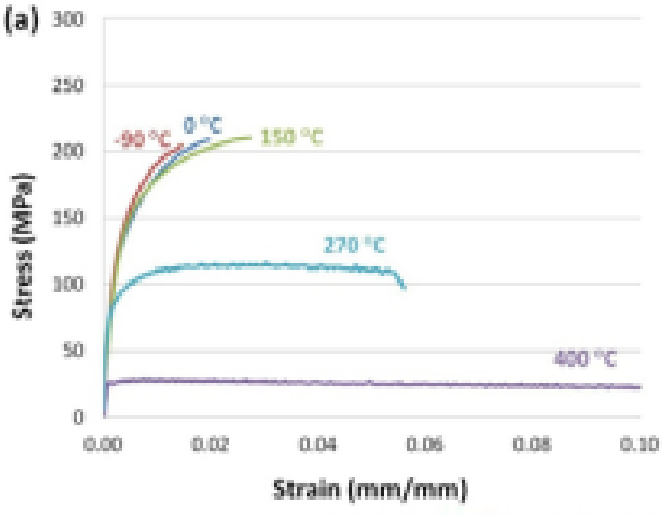


Figure 3.10: Stress-strain curve at various temperatures [8]

Figure 3.10 shows a similar trend as obtained in this study. The stress decreases as the temperature increases but the strain continue to increase as the temperature increases. This is due to the atoms of impurities that are intercepted by moving dislocations, immobilized and abruptly released. Stopping dislocation movement will results the stress to increase, while release of dislocation causes stress to decrease. At low speed, the strain increment caused by the stress increment is slow and once it reaches enough value for dislocation release, the fast plastic flow phase starts, causing the stress decrease [9].

It is important to note that the chemical composition have many different types of intermetallic that evolved during the solidification. Differences of cooling rate when the material

was manufactured results in variability in grain size and grain morphology. Both of these factor will affect the mechanical properties of the material. [8]

How the material was heat treated and the cooling rate clearly has the impact on the result obtained in this study. We can see that al 7 series has the highest stress when exrted with high temperature, this is due to the nature that AL 7075-T6 was artificially aged which requires low temperature and longer time which in turn produces a stronger material.

## 4.0: CONCLUSION

This study has showed that Aluminum 1100-O, 2024-T4 and 7075-T6 is a temperature dependent material where the thermal stress exerted is indirectly proportional to the temperature while the thermal strain is directly proportional to the temperature. This study has concluded that Aluminum 7 series is the most suitable material to be used for aircrafts nacelle lip skin since it has highest tensile yield strength hence it has ability to withstand higher stress without deforming plastically.

## REFERENCES


[1] Civil Aviation Authority, “Aircraft Icing Handbook,” no. 1998, pp. 1–108, 2000.

[2] M. A. Ismail and M. Z. Abdullah, “Applying Computational Fluid Dynamic to Predict the Thermal Performance of the Nacelle Anti-Icing System in Real Flight Scenarios,” *Indian J. Sci. Technol.*, vol. 8, no. 30, Nov. 2015.

[3] C. Sreedharan, Q. H. Nagpurwala, and S. Subbaramu, “Effect of Hot Air Jets from a Piccolo Tube in Aircraft Wing Anti-Icing Unit,” *MSRUAS-SASTech J.*, vol. 13, no. 2, pp. 2–5, 2014.

[4] S. Kennedy, T. Robinson, and S. Spence, “The Effect of Lipskin Damage on Inlet Distortion,” *Aiaa*, no. January, pp. 1–15, 2010.

[5] “ANSYS Fluent Theory Guide,” vol. 15317, no. November, pp. 724–746, 2013.

[6] A. You, “Aircraft Deicing and Anti-icing Equipment,” *AOPA Air Saf. Found.*, 2004.

[7] ANSYS Inc., “ANSYS Mechanical User’s Guide,” *ANSYS Man.*, vol. 15317, no. February, pp. 724–746, 2014.

[8] J. B. Ferguson, H. Lopez, K. Cho, and C.-S. Kim, “Temperature Effects on the Tensile Properties of Precipitation-Hardened Al-Mg-Cu-Si Alloys,” *Metals (Basel).*, vol. 6, no. 3, p. 43, 2016.

[9] A. Lipski and S. Mrozinski, “The effects of temperature on the strength properties of aluminium alloy 2024-T3,” *Acta Mech. Autom.*, vol. 6, no. 3, pp. 62–66, 2012.

**APPENDICES**

| Mass Flow Rate (Kg/s) | $Re_G$ | $Nu_{ave}$ | $Nu_{Brown}$ |
|---|---|---|---|
| 0.004596291 | 91.4516 | 19.5352 | 58.9123 |
| 0.00685458 | 136.3844 | 35.4375 | 87.5772 |
| 0.009112869 | 181.3172 | 49.522 | 116.1652 |
| 0.011371158 | 226.25 | 64.0441 | 144.696 |
| 0.013629447 | 271.1828 | 81.8369 | 173.1812 |
| 0.015887736 | 316.1156 | 95.6854 | 201.6284 |
| 0.018146025 | 361.0483 | 107.6281 | 230.4298 |
| 0.020404314 | 405.9811 | 121.9676 | 258.4298 |
| 0.022662603 | 450.9139 | 137.2291 | 286.7911 |
| 0.024920892 | 495.8468 | 153.9968 | 315.1297 |

Table 2.1: Data obtained from the CFD simulation

| Property | Value | | |
|---|---|---|---|
| | AL 1100-O | AL 2024-T4 | AL 7075-T6 |
| Density ($Kg/m^3$) | 2707 | 2785 | 2804 |
| Coefficient of Thermal Expansion at 20°C (1/°C) | 2.3600E-05 | 2.2800E-05 | 2.3200E-05 |
| Young's Modulus (Pa) | 6.8900E+10 | 7.3100E+10 | 7.1700E+10 |
| Poisson's Ratio | 0.33 | 0.33 | 0.33 |
| Bulk Modulus (Pa) | 6.7549E+10 | 7.1667E+10 | 7.0294E+10 |
| Shear Modulus (Pa) | 2.5902E+10 | 2.7481E+10 | 2.6955E+10 |
| Tensile Yield Strength (Mpa) | 110 | 324 | 503 |
| Tensile Ultimate Strength (Mpa) | 124 | 469 | 572 |

Table 2.2: Properties of the Aluminum sued in Ansys Mechanical

| Re G | 1 Series | | 2 Series | | 7 Series | |
|---|---|---|---|---|---|---|
| | **Stress** | **Strain** | **Stress** | **Strain** | **Stress** | **Strain** |
| **68.5887** | 8.9092E+05 | 3.2490E-04 | 9.1319E+05 | 3.1389E-04 | 9.1142E+05 | 3.1939E-04 |
| **102.2883** | 4.0281E+06 | 8.2031E-04 | 4.1288E+06 | 7.9250E-04 | 4.1208E+06 | 8.0640E-04 |
| **135.9879** | 4.6122E+06 | 1.3043E-03 | 4.7274E+06 | 1.2601E-03 | 4.3202E+06 | 1.2822E-03 |
| **169.6875** | 4.2230E+06 | 1.8451E-03 | 4.3286E+06 | 1.7826E-03 | 4.2377E+06 | 1.8138E-03 |
| **203.3871** | 4.1425E+06 | 2.5965E-03 | 4.2460E+06 | 2.5085E-03 | 3.8976E+06 | 2.5525E-03 |
| **237.0867** | 3.8100E+06 | 3.0258E-03 | 3.9052E+06 | 2.9232E-03 | 3.3596E+06 | 2.9745E-03 |
| **270.7863** | 3.2841E+06 | 3.3086E-03 | 3.3662E+06 | 3.1965E-03 | 3.3596E+06 | 3.2526E-03 |
| **304.4859** | 3.2416E+06 | 3.3905E-03 | 3.3226E+06 | 3.2756E-03 | 3.3162E+06 | 3.3331E-03 |
| **338.1855** | 3.0831E+06 | 3.4235E-03 | 3.1602E+06 | 3.3075E-03 | 3.1540E+06 | 3.3655E-03 |
| **371.8851** | 3.3096E+06 | 3.6194E-03 | 3.3924E+06 | 3.4967E-03 | 3.3856E+06 | 3.5581E-03 |

Table 3.1: Table of average stress and average strain for constituent Reynold number

| Re G | Maximum Temp °C | 1 Series | 2 Series | 7 Series | 1 Series | 2 Series | 7 Series |
|---|---|---|---|---|---|---|---|
| | | Max Stress | Max Stress | Max Stress | Max Strain | Max Strain | Max Strain |
| **68.5887** | 39.845 | 2.9670E+06 | 3.0411E+06 | 3.0352E+06 | 3.6331E-04 | 3.5099E-04 | 3.5372E-04 |
| **102.2883** | 65.27 | 1.2081E+07 | 1.2383E+07 | 1.2359E+07 | 9.6988E-04 | 9.3700E-04 | 9.5344E-04 |
| **135.9879** | 90.76 | 1.3162E+07 | 1.3491E+07 | 1.3465E+07 | 1.4829E-03 | 1.4327E-03 | 1.4578E-03 |
| **169.6875** | 117.654 | 9.3717E+06 | 9.6060E+06 | 9.5873E+06 | 2.0113E-03 | 1.9431E-03 | 1.9772E-03 |
| **203.3871** | 148.395 | 7.7239E+06 | 7.9169E+06 | 7.9015E+06 | 2.7579E-03 | 2.6644E-03 | 2.7111E-03 |
| **237.0867** | 167.208 | 7.6010E+06 | 7.7910E+06 | 7.7758E+06 | 3.1681E-03 | 3.0607E-03 | 3.1144E-03 |
| **270.7863** | 174.816 | 6.3454E+06 | 6.5040E+06 | 6.4914E+06 | 3.4311E-03 | 3.3148E-03 | 3.3729E-03 |
| **304.4859** | 176.585 | 6.0762E+06 | 6.2280E+06 | 6.2159E+06 | 3.5098E-03 | 3.3908E-03 | 3.4503E-03 |
| **338.1855** | 178.68 | 5.6718E+06 | 5.8136E+06 | 5.8023E+06 | 3.5350E-03 | 3.4151E-03 | 3.4751E-03 |
| **371.8851** | 186.913 | 5.9507E+06 | 6.0990E+06 | 6.0876E+06 | 3.7415E-03 | 3.6146E-03 | 3.6781E-03 |

Table 3.2: Table of maximum temperature against maximum stress and maximum strain